AZO/Ag/AZO anode for resonant cavity red, blue, and yellow organic light emitting diodes

A. R. Gentle, S. D. Yambem, P. L. Burn, P. Meredith, and G. B. Smith

---

Articles you may be interested in

The influence of MoOx gap states on hole injection from aluminum doped zinc oxide with nanoscale MoOx surface layer anodes for organic light emitting diodes
J. Appl. Phys. **118**, 065304 (2015); 10.1063/1.4928171

Aluminum-doped zinc oxide formed by atomic layer deposition for use as anodes in organic light emitting diodes
J. Vac. Sci. Technol. A **31**, 01A101 (2013); 10.1116/1.4738749

The properties of tris (8-hydroxyquinoline) aluminum organic light emitting diode with undoped zinc oxide anode layer
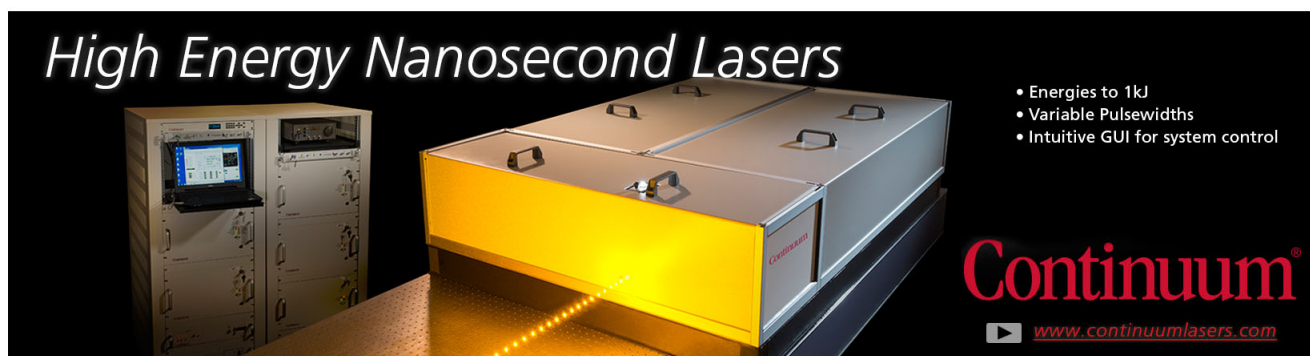J. Appl. Phys. **108**, 064518 (2010); 10.1063/1.3486058

Indium-free transparent organic light emitting diodes with Al doped ZnO electrodes grown by atomic layer and pulsed laser deposition
Appl. Phys. Lett. **93**, 073308 (2008); 10.1063/1.2975176

Organic light emitting diodes using a Ga:ZnO anode
Appl. Phys. Lett. **92**, 193304 (2008); 10.1063/1.2917565

AZO/Ag/AZO anode for resonant cavity red, blue, and yellow organic light emitting diodes

A. R. Gentle,[1,a)] S. D. Yambem,[2,b)] P. L. Burn,[2] P. Meredith,[2] and G. B. Smith[1]

[1]*School of Mathematical and Physical Sciences and Institute of Nanoscale Technology, University of Technology Sydney, P.O. Box 123, Broadway, New South Wales 2007, Australia*
[2]*Centre for Organic Photonics and Electronics, School of Chemistry and Molecular Biosciences and School of Mathematics and Physics, The University of Queensland, St Lucia, Queensland 4072, Australia*

Indium tin oxide (ITO) is the transparent electrode of choice for organic light-emitting diodes (OLEDs). Replacing ITO for cost and performance reasons is a major drive across optoelectronics. In this work, we show that changing the transparent electrode on red, blue, and yellow OLEDs from ITO to a multilayer buffered aluminium zinc oxide/silver/aluminium zinc oxide (AZO/Ag/AZO) substantially enhances total output intensity, with better control of colour, its constancy, and intensity over the full exit hemisphere. The thin Ag containing layer induces a resonant cavity optical response of the complete device. This is tuned to the emission spectra of the emissive material while minimizing internally trapped light. A complete set of spectral intensity data is presented across the full exit hemisphere for each electrode type and each OLED colour. Emission zone modelling of output spectra at a wide range of exit angles to the normal was in excellent agreement with the experimental data and hence could, in principle, be used to check and adjust production settings. These multilayer transparent electrodes show significant potential for both eliminating indium from OLEDs and spectrally shaping the emission. *Published by AIP Publishing.*
[http://dx.doi.org/10.1063/1.4954689]

I. INTRODUCTION

The use of multilayer oxide/metal stacks as transparent conducting electrodes for both organic photovoltaic (OPV) devices and organic light-emitting diodes (OLEDs) has become a hot topic in recent years.[1–4] The growing interest in alternate transparent conducting electrodes is part of a general move away from indium tin oxide (ITO), which is a response to both a perceived future limit in indium supply, as well as issues relating to the limited flexibility of ITO electrodes. Other flexible alternatives, such as graphene and silver nanowire composites,[5,6] have been shown to work well but are less able to support the resonant behaviour that can lead to gains in output, and colour sculpting and directionality that is of interest to OLED development. Maximising power efficiency (lm/W) and desired luminance profile from an OLED requires balancing hole and electron injection and transport, optimising charge capture and exciton formation, efficient use of both singlet and triplet excitons, a high photoluminescence quantum yield of the emissive species, and maximum out-coupling of the light generated in the device. The out-coupling of light can be enhanced through device design or, as has been shown more recently, by alignment of the emissive dipoles.[7] The extraction efficiency (or light out-coupling) is especially challenging for bottom emitting devices, where the transparent

substrate is coated with the transparent conducting electrode, as this combination can trap internally a high proportion of emitted light due to total internal reflection at the substrate-air interface.[8] Top emitting devices usually have higher extraction efficiency[9] but can still trap many of the photons generated in the device. Enhancing light out-coupling is important if OLEDs are to play a significant role in lighting applications.

Sharp cavity resonances have been considered previously for sculpting the emission from OLEDs.[10] Their ability to fine-tune the spectral output enables emission with better colour sharpness and purity at the spectral peak to reach the ideal C.I.E. coordinates for a particular pixel. The spatial location of the recombination/emission peak within the cavity relative to the cathode also influences the output angular spatial profile and net output,[11] and can be tuned by changing the layer thicknesses although it should be noted that this could cause a decrease in efficiency if charge injection and transport are compromised. The use of cavity resonances for emission tuning is less prominent for thick transparent electrodes with relatively low refractive indices. In these latter cases, external optics is needed to extract more light and to alter output profile.

Here, we compare the use of aluminium zinc oxide/silver/aluminium zinc oxide (AZO/Ag/AZO—defined as OSO) electrodes with the more typically used indium tin oxide transparent conducting electrode. Following a recently proposed model of the charge activated emission zone,[11] we report optimized designs for devices composed of solution processed light-emitting polymers that emit blue, yellow, or red light. The type of electrode was found to have a profound

---

a)Author to whom correspondence should be addressed. Electronic mail: angus.gentle@uts.edu.au
b)Present address: Chemistry, Physics, Mechanical Engineering, Biomedical Engineering and Medical Physics, Queensland University of Technology, GPO Box 2434, Brisbane, Queensland 4000, Australia.

impact on all key aspects of device output with the OSO multilayer electrodes enabling tuning of the spectral response and the associated angular luminance profile for each different colour. Additional benefits of the OSO electrodes are higher flexibility than ITO, and room-temperature deposition allowing fabrication on flexible polymer substrates. The silver layer that is between the two AZO layers provides the lateral conductivity, while the oxide layers provide the required optical impedance matching for transparency to allow effective out coupling of light.

II. EXPERIMENTAL SECTION

A. Materials and fabrication

1. OSO electrode fabrication

The AZO and Ag layers of the electrode were deposited at room temperature using DC magnetron sputtering from a target consisting of ZnO doped with 2% Al with a shadow mask to produce the electrode pattern. Substrates were 25 mm square glass and Dupont Teonex® Q65FA polyethylene naphthalate (PEN) substrates. 2 in. Sputter targets were used with a base chamber pressure of 1×10^{-6} Torr, with argon introduced at a pressure of 1.5 mTorr. The AZO and Ag layers were deposited with a 0.2 A and a 0.1 A current, respectively. The target to sample working distance was 150 mm. A rotating sample stage ensured thickness uniformity of each layer across the substrate. The rotating sample stage was directed off the central axis of the substrate by 100 mm to increase the conductivity of the thin AZO film AZO.[12] The optimum position of the sample stage in relation to the AZO target was determined using a non-rotating large glass sample. The position of highest conductivity was then set as the central position of the substrate. The thickness of the silver layer is chosen such that a smooth transparent conductive layer is deposited. If the thickness of the silver is reduced, parasitic plasmonic absorption occurs due to the percolating silver structure. The thicknesses of the oxide are chosen to maximize light out coupling as described in Section III.

2. Device fabrication

All the device fabrication steps were carried out inside a nitrogen glove box ($O_2 < 0.1$ ppm, $H_2O < 0.1$ ppm). In addition to the 8.4 Ω/sq-3 nm AZO/11.5 nm Ag/10 nm AZO multilayer stack electrodes, standard 15 Ω/sq ITO substrates were also used. The ITO substrates purchased from Xinyan Technology were cleaned using a lint free swab in a solution of Alconox in deionised water, followed by rinsing several times in deionised water, and ultrasonication in deionised water, acetone, and 2-propanol for 10 min each. After cleaning of the substrates, a 10 nm thick MoOx layer was deposited via thermal evaporation onto both electrode types simultaneously. The emissive materials were purchased from Merck and dissolved in filtered toluene (anhydrous grade) at the following concentrations: super yellow (PDY-132) (5 mg/ml), polymer blue (SPB-02 T) (8 mg/ml), polymer red (SPR-001) (13 mg/ml) by stirring overnight at room temperature prior to device fabrication. The emissive layers were

deposited by spin-coating using the following parameters: super yellow—1000 rpm for 60 s, polymer red—1200 rpm for 60 s, and polymer blue—1300 rpm for 60 s. The spin rates for the desired thicknesses were calibrated via ellipsometric measurements of reference samples spin-coated onto silicon with a native oxide. The devices were then completed by cathode deposition by thermal evaporation through a shadow mask. Each of the six devices on each substrate had an active area of 20 mm^2, which was defined using a shadow mask. The cathode consisted of a thin ($\approx$4.6 nm) barium layer capped with a thick (100 nm) aluminium top contact.

B. Characterisation

Current-voltage-luminance (IVL) measurements of the OLEDs were carried out using an Agilent B1500A semiconductor device analyzer and a calibrated photodiode positioned such that the majority of the hemisphere emission was captured. Angular spectral output measurements were taken using a goniometer mounted Ocean Optics USB2000 spectrometer mounted with a 25 mm lens for light collection at a rotational working distance of 470 mm giving a collection solid angle of approximately 3°. In order to evaluate the outcoupling of the OLEDs, spectral measurements were taken at 1° intervals over the same one axis of the hemisphere for each different OLED studied. Optical properties of all films were characterised via ellipsometry using a J.A. Woollam V-VASE ellipsometer. Samples were measured at 65°, 70°, and 75° incidence between 300 and 2500 nm. Optical constants were fitted using oscillator models to ensure Kramers–Kronig consistency is maintained.

III. RESULTS AND DISCUSSION

The architectures of the two bottom emitting OLEDs are shown in Figure 1 and are composed of: glass/3 nm AZO/11.5 nm Ag/10 nm AZO/10 nm MoOx/OLED active layer/Ba/Al and glass/23 nm SiO$_2$/82 nm ITO/10 nm MoOx/OLED active layer/4.6 nm Ba/100 nm Al, with the emissive layer thicknesses shown in Table I.

The role of the very thin AZO layer ($\sim$3 nm) beneath the silver is to act as a wetting layer to assist the percolation
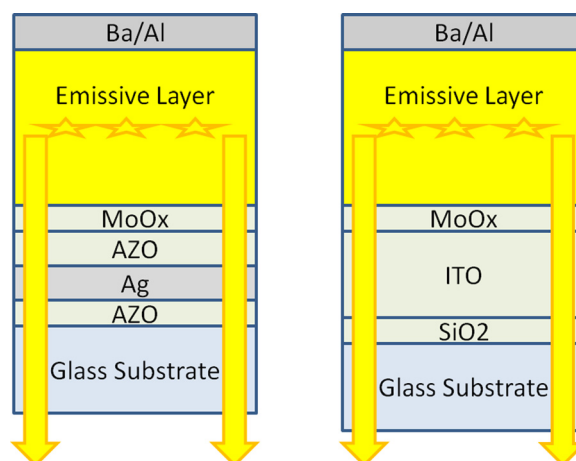

FIG. 1. Schematic of the two bottom emitting OLED systems that are compared (not to scale).

TABLE I. OLED emissive layer thickness (optimised thicknesses in brackets).

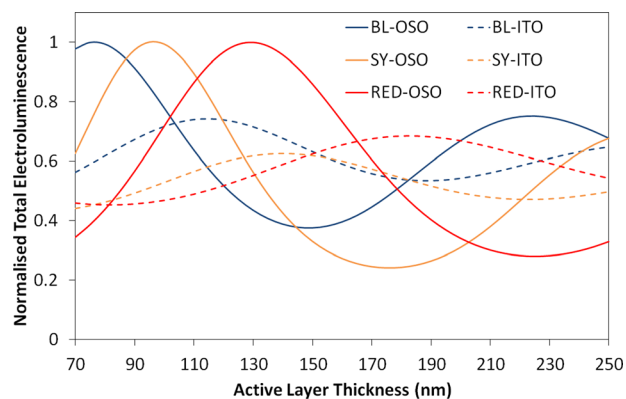| Electrode type	Super yellow (nm)	Red (nm)	Blue (nm)
AZO stack	(90), 110	110, (130)	(105), 200
ITO	(90), 110	110, (130)	(105), 110

FIG. 2. Modelled effect of active layer thickness (blue, red, and super yellow) on integrated light output, for devices made with OSO and ITO electrodes.

of the silver. As noted previously,[12] an advantage of AZO based stacks compared to other sandwich oxide stacks such as MoOx-Ag-MoOx is that the wetting of Ag on AZO maximises conductivity, increases transmittance, and minimises parasitic plasmonic absorption. The thicknesses of the second layer of AZO and the emissive layer were the variables that were used to tune the cavity resonance. The thickness of the second AZO layer was adjusted such that to first order it would work sufficiently well in terms of transparency with each different polymer. Thus, the emissive layer thickness was varied to maximise the cavity out-coupling, rather than having separate optimised electrodes for each colour. The addition of the MoOx layer on top of the OSO stack was to tune the work function of the anode in an effort to achieve an ohmic contact with the polymer layers.[12–15] The MoOx layer was thin to avoid unwanted series resistance in the devices and was deposited just before use to avoid air exposure and changes to the work function[14] which we observe when MoOx is exposed to air over a period of time.

In such devices, the light extraction efficiency can be enhanced if the total outgoing transmittance of the active layer-transparent electrode-substrate combination is highest at wavelengths where emitted photons are plentiful. That is, the optical response of the whole device and the electroluminescence should be in resonance for the best out-coupling of the light. Thus, the ideal electrodes may appear to have a relatively high reflectance when measured in air, but when coupled with the active layer and counter electrode will perform better than traditional transparent electrodes using "in-air" traditional figure of merits.

Transparent conducting electrodes of the type oxide/metal/oxide are ideal for achieving high Q cavity resonances to maximise output, because each layer is a thin film and the metal layer dielectric constant is highly dispersive. In combination with its antireflection oxide layers, optical impedance dispersion is much stronger than that in thick, metal free transparent conducting electrodes such as ITO. Considerable spectral variation in the effective complex dielectric constant of the transparent electrode is needed to establish a strong cavity resonance between it and the opposite aluminium electrode over a desired range of wavelengths.[12] In contrast, the thicker ITO electrodes rely on an almost constant refractive index and low absorption coefficient for their transparency. They thus yield a weaker and broader (or low Q) resonance effect as we shall now demonstrate and discuss. We first use the emission zone method presented by Epstein *et al.*[11] to model and optimise the efficiency of OLEDs whose transparent electrode is either the AZO/Ag/AZO/MoOx four layer stack or an ITO/MoOx bilayer. To understand the efficiency and colour tuning effects, we then use the direction dependent spectral emission OLED device modelling in the range of emission directions

from the normal to nearly ±90°. In both cases, we use the total electrode structure in the modelling, although the effect is greatest for the thinner AZO/Ag/AZO/MoOx four layer stack electrode (Figure 2). The effective impedance of the electrode stack is dependent on the structure, with the wavelength dependence of the impedance along with the thickness of the resonant cavity enabling fine tuning to maximise total output intensity and control of the emission profile. This is due to its impact on the sensitivity of change of optical output to emission layer thickness (Figure 2).

The results shown in Figure 3 are presented for the optimized devices, prepared and measured as discussed in Sections II A 1 and II A 2. Additional detailed current-voltage-luminance (IVL) and external quantum efficiency (EQE) plots can be found in the supplementary material.[16] It can be seen in Tables II and III that only at very low lumens output does the blue emitter with an OSO electrode have lower EQE than that with the ITO electrode. However, the low bias luminance is still higher for blue. The reason for this is as follows. The two have similar spectral responses at blue wavelengths, but the OSO electrode yields a much different and stronger output at green wavelengths with an additional peak not seen in the ITO case. Since the eye is more sensitive to green than blue, more lumens and higher luminance result with OSO than ITO.

A qualitatively similar comparison in terms of output spectral shape is seen for the red emitter. Though similar in
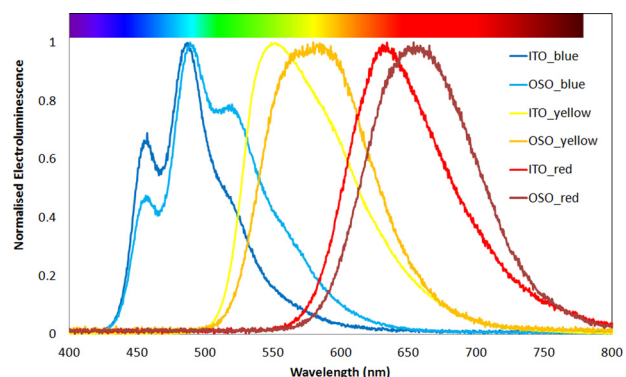

FIG. 3. Normalised electroluminescence spectrum of the six devices.

TABLE II. Device EQE at different brightness.

Device	EQE at 100 cd/m^2	EQE at 1000 cd/m^2	EQE at 10 000 cd/m^2
ITO/SY	1.59 ± 0.07 (1.66)	2.30 ± 0.07 (2.38)	2.15 ± 0.10 (2.27)
OSO/SY	2.18 ± 0.13 (2.35)	3.11 ± 0.14 (3.24)	3.08 ± 0.03 (3.14)
ITO/red	1.98 ± 0.10 (2.09)	1.56 ± 0.04 (1.61)	…
OSO/red	2.56 ± 0.13 (2.72)	1.96 ± 0.12 (2.15)	…
ITO/blue	1.29 ± 0.07 (1.37)	1.57 ± 0.03 (1.60)	…
OSO/blue	1.03 ± 0.16 (1.20)	1.60 ± 0.11 (1.75)	…

Standard deviations are calculated for six devices for each device type. (The values in the parentheses represent highest EQE at the respective brightness.)

emission to ITO below 650 nm, the EQE is very much higher with the OSO electrode at wavelengths from 650 nm to where the visible response ends. This means that a much purer "red" is produced with an OSO electrode. The strong resonant effect for blue and red relative to what is observed with ITO are similar in peak broadening terms. While this added spectral density meant more lumens for the blue emission, as noted above, for red such additions are in regions where the eye sensitivity continues to drop so for the OSO case red lumens and average luminance are lower than with ITO. It is associated with a shift of the OSO peak output to 670 nm from the 630 nm peak position seen with ITO. This lower red luminance with OSO only occurs at lower voltages. Once a normal large transfer injection occurs at higher V, many extra OSO based red photons are emitted relative to those with ITO at all output wavelengths as in Figure 3. Then both higher EQE and higher luminance occur. The colour of each device can be seen in Table IV and Figure 4, including the ability to tune the OSO device emission colour via active layer thickness. Thus, devices can be optimised for output colour or intensity as done in this case. A full set of electroluminescence current/voltage/luminance and EQE curves are available in the supplementary material.[16] The supplementary material shows that similar threshold biases are seen for both the ITO and OSO electrodes, indicating that differences in devices performance cannot be attributed to differences in charge injection.

It can be seen in Figure 4 that by tuning the thickness of the resonant cavity via varying the active layer thickness, it is possible to use the same electrode to efficiently extract photons over a broader wavelength range than with the ITO electrode. This is possible because the thickness for each different colour emitter thickness can be chosen individually to tune the cavity to maximize the output for the desired wavelengths.

Using a similar 4-layer electrode system to our recently published work on OPVs,[12] we have re-tuned the stack

TABLE IV. Normal incidence CIE co-ordinates.

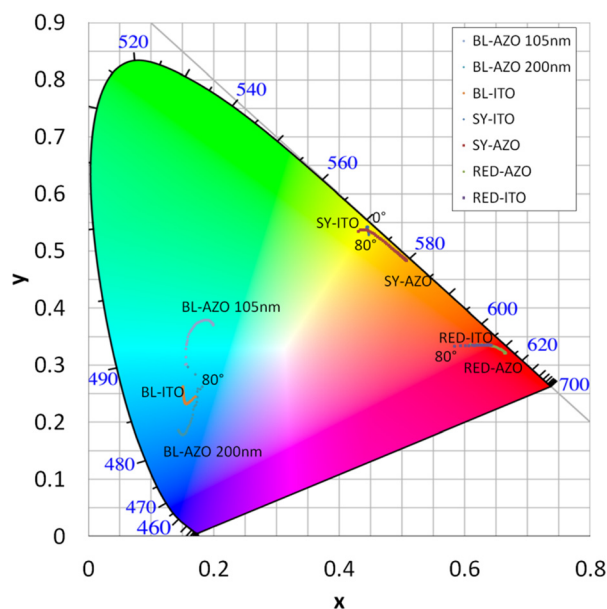| Device	X	Y
ITO/SY	0.450	0.539
OSO/SY	0.497	0.488
ITO/blue	0.155	0.282
OSO/blue	0.205	0.416
ITO/red	0.647	0.335
OSO/red	0.652	0.320

FIG. 4. CIE 1931 colour map of the device results showing the range of emission colours (BL = blue, SY = super yellow, RED) produced from the normal to the OLED to 80° to its normal. For BL-AZO, the thickness indicates that of the active layer.

design for use in OLEDs. In order to maximise the out-coupling profiles for red, blue, and yellow, we utilised the Epstein Emission Zone technique.[11] To optimise the stack, we reconfigured the Matlab script to allow for looping though the various thickness combinations to identify the desired thicknesses for each layer in the electrode and for the active emitter layer. This study focuses on bottom emitting devices, in which the light is emitted through the glass substrate.

The sensitivity of output intensity to cavity thickness, as summarised in the theoretical plots of Figure 2, is demonstrated experimentally in a sequence of images which display a contour plot of intensity as a function of exit direction and exit wavelength, and can be found in the supplementary material.[16] Each plot is for a different thickness of active layer.

TABLE III. Luminance (cd/m^2) for each device type for an applied bias of 3, 5, and 10 V.

Voltage (V)	ITO/SY	OSO/SY	ITO/Red	OSO/Red	ITO/Blue	OSO/Blue
3	48 ± 7 (57)	62 ± 6 (75)	12 ± 1 (13)	10 ± 1 (11)	2 ± 0 (2)	4 ± 1 (5)
5	1201 ± 173 (1430)	1471 ± 127 (1743)	170 ± 11 (179)	125 ± 10 (133)	210 ± 14 (223)	323 ± 49 (381)
10	12 783 ± 1523 (15 096)	25 447 ± 2012 (29 243)	1805 ± 203 (2186)	1836 ± 147 (1954)	3394 ± 363 (3870)	6646 ± 963 (7570)

Standard deviations are calculated for six devices for each device type. (The values in the parentheses represent highest luminance at the respective voltage.)

Subsequent precise modelling of the MoOx buffered OSO based electrode films used for our initial devices indicated that there was considerable scope for improvement on earlier samples by changing the emissive layer thickness. These models, described below, were first tested against the early experimental data for their ability to accurately predict the spectral variation of output. Later validation was extended to their ability to predict observed emission intensity and spectral response over the full exit hemisphere.

The reliability of light output modelling as a predictor of experimental performance having been proven for multilayer electrodes enabled us to pre-determine the optimum thicknesses of the emitting layer. Then we could assess after production if a given device had been produced as structurally intended or if the production process could be further improved. The models also allowed accurate prediction of intensity at any exit angle and hence of the expected lm m^{-2}Sr^{-1} in each direction, that is, the output luminance profile.

It is apparent that peak wavelengths, spectral shape, and wavelength span differ for the same active layer with an AZO/Ag/AZO multilayer and ITO based electrodes. Such differences lead to distinct differences in output colour and hence colour rendering for the same emissive molecule along with different net lumens, and lumens/Watt emitted. The thin multilayer electrode yields superior overall performance, as well as the ability to tune the colour of the output. External quantum efficiency and output luminance are quantified in Tables II and III where it is clear that very large gains in key measures arise when ITO is replaced with OSO stack electrodes.

IV. ANGULAR SPECTRAL RESPONSE

A. Data

External to the device, the quality of light available for a particular task depends not just on lumens produced but on the spatial spread of that light. That is the luminance as a function of exit angle is important. Internally, the angular response not only influences the external distribution but also the amount of light that does not escape, hence net lumens.

Despite utilising a resonant cavity effect to maximise light out-coupling, light output is not necessarily restrained to angles closer to the normal. This occurs because the resonant cavity design can be chosen to maintain a larger viewing angle than that with the standard ITO devices. Unlike micro-cavity OLEDs which suffer from significant colour shifts with viewing angle,[17] our resonant cavity which is formed between the silver in the anode and the aluminium cathode layer (separated by 80–140 nm active layer), if designed carefully does not suffer as severely from the same problem. This was verified with optical modelling of the device stacks and then confirmed with experimental data.

Observing the measured normalised angular spectral emission intensity maps shown in Figures 5–7 covering yellow, blue, and red emitters each with OSO and ITO electrodes, of particular interest is the differences in spectral and angular emission between the two electrode types as predicted by the modelling.

For blue and yellow emitters, the high intensity zone clearly extends over a much wider range in terms of both
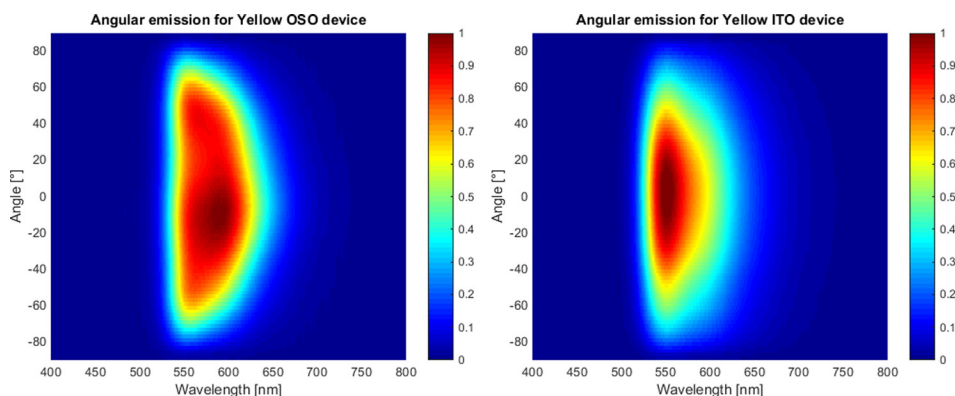

FIG. 5. Measured intensity contours in spectral and angular 2-dimensional space for 90 nm yellow emitter with OSO and ITO electrodes. The colour bar represents the normalised electroluminescent intensity.
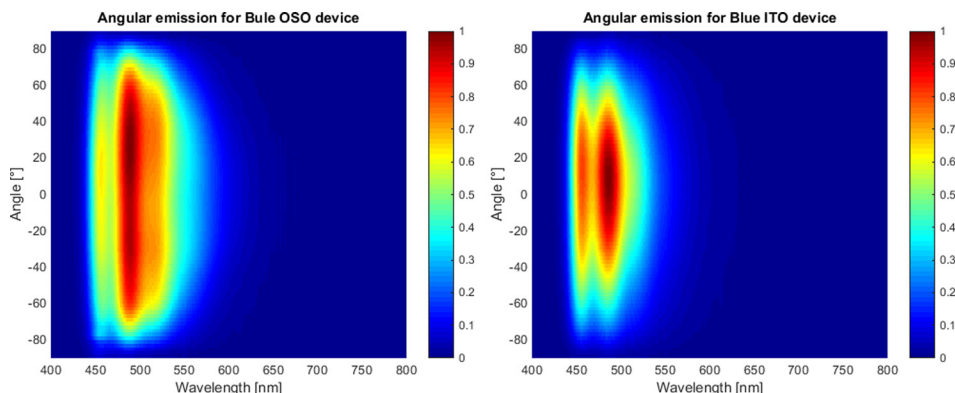

FIG. 6. Measured intensity contours in spectral and angular 2-dimensional space for 105 nm blue emitter with OSO and ITO electrodes. The colour bar represents the normalised electroluminescent intensity.
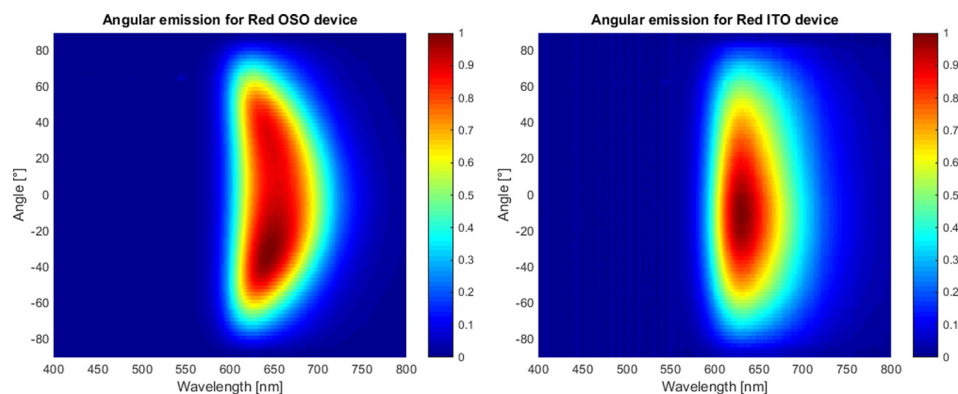
FIG. 7. Measured intensity contours in spectral and angular 2-dimensional space for 130 nm red emitter with OSO and ITO electrodes. The colour bar represents the normalised electroluminescent intensity.
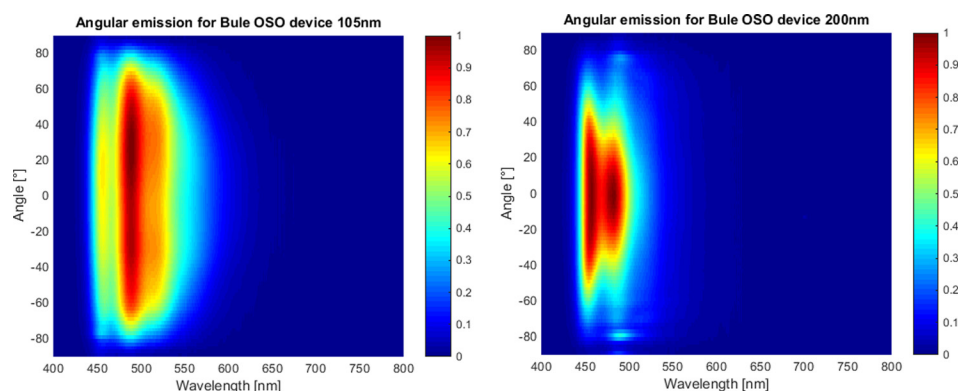

FIG. 8. Measured intensity contours in spectral and angular 2-dimensional space demonstrating colour shift due to blue active layer thickness tuning of the OSO device resonant cavity by varying the active layer thickness from 105 nm to 200 nm. The colour bar represents the normalised electroluminescent intensity.
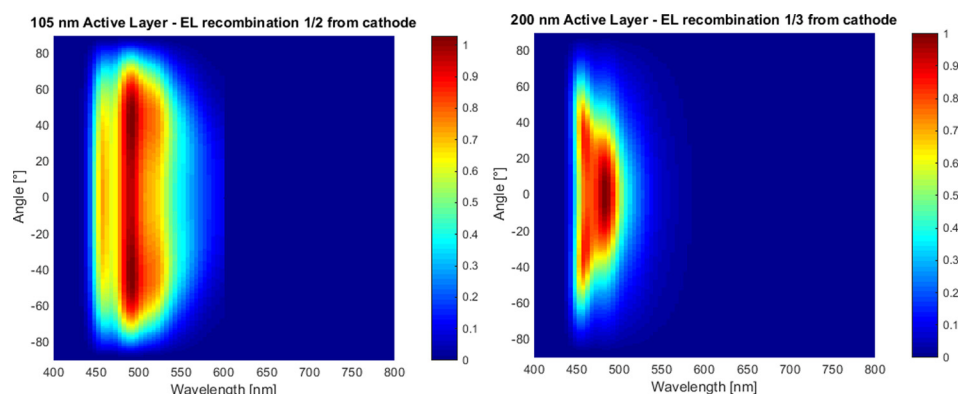

FIG. 9. Modelled intensity contours in spectral and angular 2-dimensional space demonstrating colour shift due to blue active layer thickness tuning of the OSO device resonant cavity by varying the active layer thickness from 105 nm to 200 nm. The colour bar represents the normalised electroluminescent intensity.

viewing cone to the normal and spectral spread. The central point of this high intensity zone for yellow and blue is in addition shifted to longer wavelengths. The position of this peak can be tuned via altering the thickness of the active layer.

An example of colour and direction control using the OSO stack design is demonstrated in Figures 8 and 9, in which the two devices have different stack designs for the blue active layer thicknesses of 105 nm and 200 nm. Significant shifts are apparent in the location of the spectral peak and output spread, resulting from the cavity resonance characteristics when active layer thickness is changed. Additionally, it demonstrates the need for considering the full hemisphere of emission rather than just normal incidence response. Figure 9 shows that the theoretical predictions are an excellent guide to data as shown in Figure 8. Sections IV B and V outline in more detail with more examples the required model inputs, their acquisition and use.

B. Optical modelling of angle and spectral dependence of emission

Refractive index data and the thicknesses of each layer, both determined via ellipsometry, are used as input values for the emission zone modelling of the output spectral response as a function of exit direction to the device normal. To determine the inherent internal emission of the OLED material, the measured emission data from the ITO device were de-convolved from the modelled product of the image source transmission and cavity mode terms at normal incidence and then used to model the emission profile of the AZO stack devices. Once the satisfactory emission spectra for the OLED material are obtained, it is then possible to model device output for arbitrary device structures. Sweeping through the active layer thickness allows for easy identification of optimal active layer thicknesses. Figure 10 shows observed spectral and angular results for two
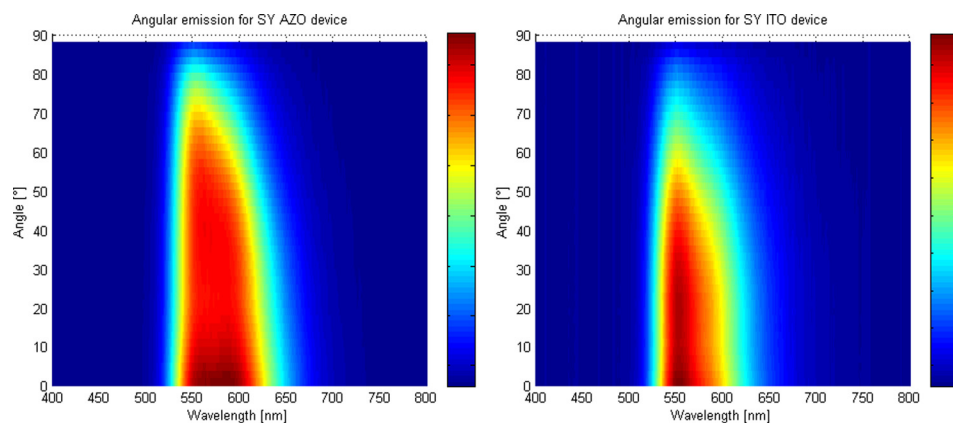
FIG. 10. Observed normalised peak angular and spectral emission from super yellow devices (left) with OSO stack at 5.7 V bias. (right) is ITO electrodes at 7 V bias. Both were measured externally. The colour bar represents the normalised electroluminescent intensity.
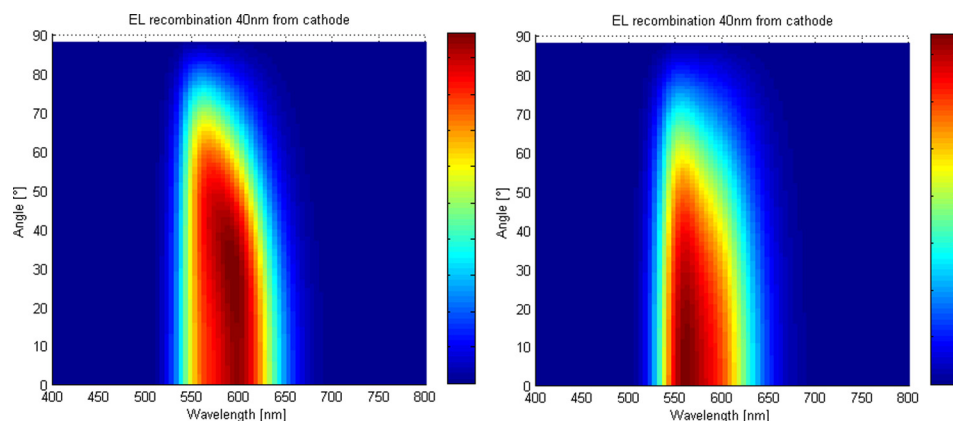

FIG. 11. Modelled normalised peak angular and spectral emission emission from super yellow devices (left) OSO stack, (right) ITO electrodes. These are as expected externally for a specific peak location of electroluminescence emission relative to the cathode. The colour bar represents the normalised electroluminescent intensity.

super-yellow OLEDs on OSO and ITO electrodes and Figure 11 the modelled results for the same structures.

Comparing the overall shape of the measured and modelled emission spectra for the AZO stack and ITO based devices in Figures 10 and 11, the AZO based devices clearly have a broader more uniform spectral shape, while the ITO devices have a higher bias towards shorter wavelength. Both modelled spectra use the same emission spectra for the active layer material, with the differences in spectral output solely dependent on the internal transmission and resonant cavity effects of the devices. To demonstrate the power of this technique, the modelled results for the two different thickness blue OSO devices are shown in Figure 9, as can be seen there is excellent agreement between modelled and measured (Figure 8) emission spectra.

V. SUMMARY AND CONCLUSIONS

In this paper, we have shown that oxide-semiconductor-oxide transparent stacks based upon AZO/Ag/AZO can be used to control the spectral and spatial profiles of emission from simple red, green, and blue organic light emitting diodes. Design tuning using Epstein's emission zone modelling in combination with appropriate knowledge of the device optical constants allows the out-coupling to be predicted and maximized. The resonant cavity effect enabled by these electrodes causes emissions over a wider range of output wavelengths and a wider range of viewing angles than with buffered ITO. In combination, this results in a higher light output for the non-ITO devices. That is a tuned cavity mode enhances the EQE by two means; a wider

spectral span of output light and the extra photons that are not trapped internally but instead emitted at higher angles. The effectiveness of the use of Epstein's[11] emission zone model for optimisation of resonant cavity OLEDs has been demonstrated. It allows for a quick and reliable simulation of expected device output for any device design contemplated. This also provides a benchmark for checking experimentally if produced devices have the intended structures, or if deposition protocols need further adjustment. The optimum thicknesses for each of the AZO layers are different for use in OLEDs presented here to those used for OPV,[12] or that for maximized in air transparency which requires symmetric oxide thicknesses. Thus, electrodes should be evaluated in terms of end use configuration, rather than simply in air transparency.

ACKNOWLEDGMENTS

Infrastructure Strategy to provide nano- and micro-fabrication facilities for Australia's researchers.

[1]K. Jeon, H. Youn, S. Kim, S. Shin, and M. Yang, Nanoscale Res. Lett. **7**, 253 (2012).

[2]H. Pang, Y. Yuan, Y. Zhou, J. Lian, L. Cao, J. Zhang, and X. Zhou, J. Lumin. **122–123**, 587 (2007).

[3]J. Jeong, J. Lee, and H. Kim, Electrochem. Solid-State Lett. **12**, J105 (2009).

[4]S. Ryu, J. Noh, B. Hwang, C. Kim, S. Jo, J. Kim, H. Hwang, H. Baik, H. Jeong, C. Lee, S. Song, S. Choi, and S. Park, Appl. Phys. Lett. **92**, 023306 (2008).

[5]L. Hu, H. S. Kim, J.-Y. Lee, P. Peumans, and Y. Cui, ACS Nano **4**, 2955 (2010).

[6]A. J. Stapleton, R. A. Afre, A. V. Ellis, J. G. Shapter, G. G. Andersson, J. S. Quinton, and D. A. Lewis, Sci. Technol. Adv. Mater. **14**, 035004 (2013).

[7]A. Graf, P. Liehm, C. Murawski, S. Hofmann, K. Leo, and M. C. Gather, J. Mater. Chem. C **2**, 10298 (2014).

[8]C. F. Madigan, M.-H. Lu, and J. C. Sturm, Appl. Phys. Lett. **76**, 1650 (2000).

[9]M.-H. Lu, M. S. Weaver, T. X. Zhou, M. Rothman, R. C. Kwong, M. Hack, and J. J. Brown, Appl. Phys. Lett. **81**, 3921 (2002).

[10]C.-L. Lin, H.-C. Chang, K.-C. Tien, and C.-C. Wu, Appl. Phys. Lett. **90**, 071111 (2007).

[11]A. Epstein, M. Roberts, N. Tessler, and P. D. Einziger, J. Appl. Phys. **115**, 223101 (2014).

[12]A. R. Gentle, S. D. Yambem, G. B. Smith, P. L. Burn, and P. Meredith, Phys. Status Solidi A **212**, 348 (2015).

[13]A. R. Gentle, G. B. Smith, and S. E. Watkins, Appl. Surf. Sci. **285**(Part B), 110 (2013).

[14]J. Meyer, S. Hamwi, M. Kröger, W. Kowalsky, T. Riedl, and A. Kahn, Adv. Mater. **24**, 5408 (2012).

[15]M. Kröger, S. Hamwi, J. Meyer, T. Riedl, W. Kowalsky, and A. Kahn, Appl. Phys. Lett. **95**, 123301 (2009).

[16]See supplementary material at http://dx.doi.org/10.1063/1.4954689 for full set of electroluminescence data (current/voltage/luminance, EQE curves, etc.).

[17]W. C. H. Choy and C. Y. Ho, Opt. Express **15**, 13288 (2007).